Optimal Design and Performance Analysis of Permanent Magnet Assisted Synchronous Reluctance Portable Generators

Jeihoon Baek[1], Sangshin Kwak[2]*, and Hamid A. Toliyat[3]

[1,3]*Department of Electrical & Computer Engineering, Texas A&M University, College Station, TX 77843-3128, USA*
[2]*School of Electrical and Electronics Engineering, Chung-ang University, Seoul 156-756, Korea*

In this paper, design and performance analysis of robust and inexpensive permanent magnet-assisted synchronous reluctance generators (PMa-SynRG) for tactical and commercial generator sets is studied. More specifically, the optimal design approach is investigated for minimizing volume and maximizing performance for the portable generator. In order to find optimized PMa-SynRG, stator winding configurations and rotor structures are analyzed using the lumped parameter model (LPM). After comparisons of stator windings and rotor structure by LPM, the selected stator winding and rotor structure are optimized using a differential evolution strategy (DES). Finally, output performances are verified by finite element analysis (FEA) and experimental tests. This design process is developed for the optimized design of PMa-SynRG to achieve minimum magnet and machine volume as well as maximum efficiency simultaneously.

Keywords : concentrated winding, differential evolution strategy, distributed winding, lumped parameter model, permanent magnet assisted synchronous generator

1. Introduction

Interior permanent magnet (IPM) machines can provide a large constant power-speed operation as well as high power density, as a result of magnetic torque and reluctance torque components [1-3]. However, the IPM machines require a large amount of rare-earth magnet and it increases machine cost. In addition, they suffer from inverter shutdown problems under uncontrolled generator mode operations [4, 5]. In order to overcome such disadvantages of the IPM machines to use as a generator, the permanent magnet-assisted synchronous reluctance machines (PMa-SynRM) can be a good candidate due to its low cost, high efficiency, and high reliability for military and commercial applications [6].

In this paper, the permanent magnet-assisted synchronous reluctance generators are developed with two flux barriers and permanent magnets embedded in the layer of the rotor. NdFeB permanent magnets are selected to prevent undesired demagnetization at high temperature operation. One design goal presented in this paper is to develop the optimization process from a cost point of view, by finding the minimum amount of NdFeB magnets to be used in the rotor [7]. Another objective is to obtain the proper number of stator slots per pole for two winding distributions [8]. Moreover, this paper presents an optimal design process for selected winding based 3 kW PMa-SynRG, to achieve a wide constant power speed range (CPSR), high efficiency, and good power factor using the LPM and the DES [9, 10]. Furthermore, iterative processes are performed for minimizing cogging torque and torque pulsations, until results of LPM and FEA predictions are converged.

2. Modeling of PMa-SynRG

In the *d-q* reference frame, the stator current can be represented by the *d* and *q*-axis currents and the current angle as [11].

$$I_d = I_a \cos\gamma, \; I_q = I_a \sin\gamma \tag{1}$$

where, I_a and γ is the a-phase current and the current angle of the I_a, respectively. The *d-q* reference flux linkages, λ_d and λ_q, and voltages, V_d and V_q, are given by

$$\lambda_d = L_d \cdot I_d \;\; \lambda_q = L_q \cdot I_q - \lambda_{PM} \tag{2}$$

*Corresponding author: Tel: +82-2-820-5346
Fax: +82-2-825-1584, e-mail: sskwak@cau.ac.kr

$$V_d = -\omega_r(L_q \cdot I_q - \lambda_{PM}) \quad V_q = \omega_r(L_d \cdot I_d) \qquad (3)$$

where, L_d and L_q are the d and q-axis inductances [12]. The electromagnetic torque T and output power P can be written by

$$T = \frac{3}{2}\frac{p}{2}(\lambda_d \cdot I_q - \lambda_q \cdot I_d)$$

$$= \frac{3}{2}\frac{p}{2}(\lambda_{PM} \cdot I_d + (L_d - L_q) \cdot I_d I_q) \qquad (4)$$

$$P = \omega_r \cdot T \qquad (5)$$

where, p is the number of pole pairs, λ_{PM}, ω_r denote the permanent magnet flux-linkage and the rotor angular speed.

For motoring operations, maximizing the output torque simultaneously maximizes the efficiency by finding the current angle of the operating point to obtain the maximum torque per ampere. However, operating along with the maximum torque per ampere trajectory is not sufficient to maximize the output power that can be extracted. For generating operations, there is no closed-form solution as in the motoring operations. In the vector diagram for generating the mode of operation shown in Fig. 1, the available maximum real power can be controlled by the negative I_d and the positive I_q components of the current vector. The angle δ between I_d and V_a in Fig. 1 denotes a torque angle. At a constant operating speed, the current vector has to operate at the intersection point of the maximum power per ampere trajectory with the voltage limit in the current limit circle. Maximizing the real power requires searching the current vector as a function of phase current, current angle γ, and torque angle δ. Consequently, the electrical terminal conditions and power capability at a given speed can be determined by iterative processes [13].
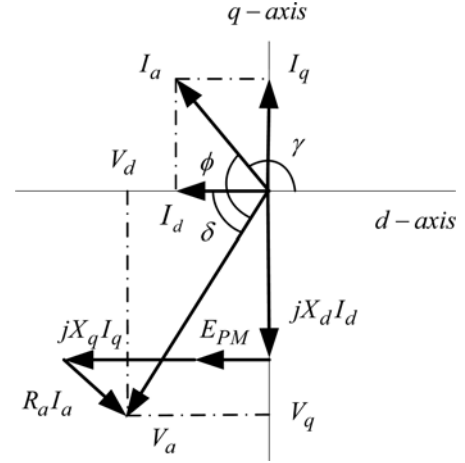

Fig. 1. Vector diagram for generating mode.

3. Proposed Optimal Design Process of PMa-SynRG using LPM, DES and FEA

3.1. Design of Rotor Structure and Stator Configurations

The rotor core for PMa-SynRG is built of conventional tran sverse laminations with stamped multiple flux barriers per pole filled with permanent magnet layers. The high magnetic saliency created by the multiple flux barriers in the rotor make reluctance torque predominant at low speeds when higher torque is required. Also, the multiple flux barriers prevent rated excitation from saturation along the q-axis of the core. Therefore, the PM flux linkage can be calculated using a linear magnetic circuit analysis similar to the q-axis inductance calculation. Fig. 2 depicts the cross-sections of PMa-SynRG and the magnetic circuit with the permanent magnet placed in the first and second layers, respectively. The first type of rotor structure in Fig. 2(a) shows that permanent magnets are inserted in the first layer and the other in Fig. 2(b) is in the second layer. The PM flux is oriented along the q-
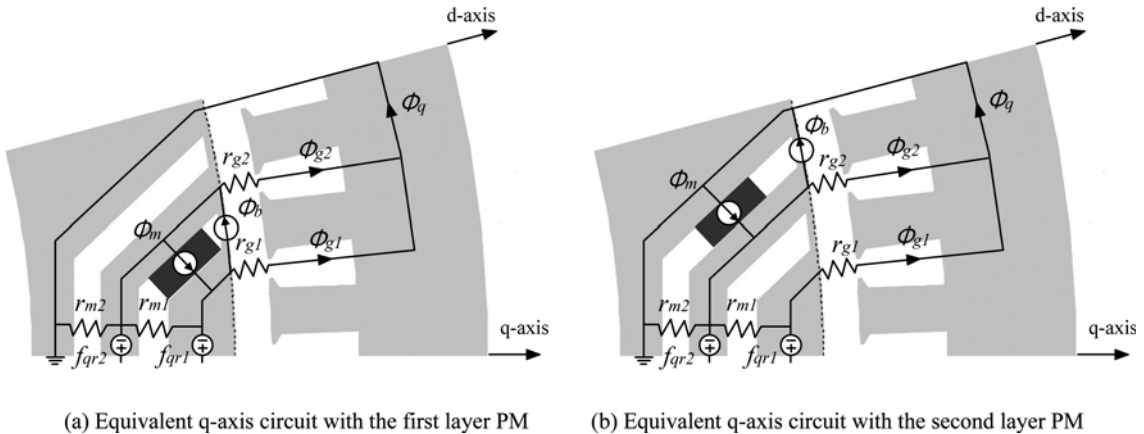
(a) Equivalent q-axis circuit with the first layer PM   (b) Equivalent q-axis circuit with the second layer PM

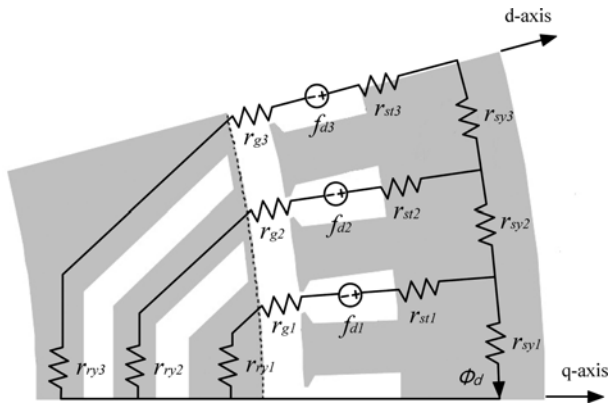**Fig. 2.** Equivalent q-axis circuit with the first and second layer PM.

Fig. 3. Nonlinear d-axis equivalent circuit.

axis, the PM flux is oriented along the q-axis, and the reluctance circuit is analyzed with the stator MMF sources removed and the flux sources added. The air-gap flux source ϕ_{gi} flows through the stator teeth, the per-unit PM flux source ϕ_m added in the PM and the estimated saturation flux source ϕ_b is in the opposite direction to the magnetic circuit.

Nonlinear saturation affects the calculation of the d-axis inductance. The nonlinear functions for the d-axis reluctances are based on the nonlinear characteristics of core material. Fig. 3 presents the nonlinear d-axis magnetic circuit and the nonlinear magnetic core characteristics are modeled by a curve fit to the B-H data of the core.

The stator winding for PMa-SynRG can be selected between distributed and concentrated windings. Based on winding configurations, the number of stator slots and rotor poles are determined. The adoption of the concentrated windings for the PMa-SynRG enables the volume of copper used in the coil end windings to be significantly reduced, compared with the conventional distributed windings. In addition, the shorter end windings provide opportunities to lower the winding copper losses and improve machine efficiency [14, 15]. However, machines with concentrated windings have higher inductances, due to higher slot leakage. Therefore, the power capabilities are quite different. Also, the distributed winding has advantages such as low EMF harmonics and torque ripple. In order to compare and select the winding configuration, the initial LPMs are developed for two different windings and the optimization process finalizes the better one.

3.2. Optimal Design using Differential Evolution Strategy

The DES, one of the genetic algorithm procedures, is suitable for finding the optimum design in nonlinear systems [16]. The DES is different from the other optimization methods such as Neural Networks and it has
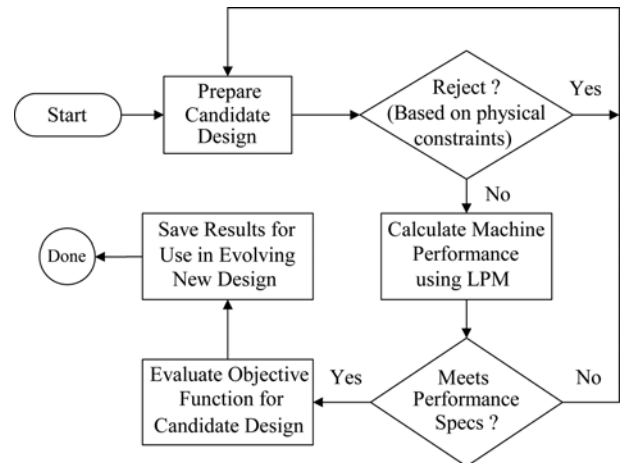

Fig. 4. Flow chart of optimization process using LPM and DES.

advantages whereby DES operates on a population of points in the search space simultaneously, not on just one point, uses the objective function, not derivatives, and is probabilistic, not deterministic. The DES is utilized in this paper to explore the multi-dimensional variable design space for the rotor structure and stator winding configuration, in order to obtain the most promising design to meet the required performance for cost and efficiency. In the flow chart illustrated in Fig. 4, the LPM generates the initial candidate design and analyzes the machine performance. In case the candidate design satisfies machine performance, the DES generates the next 10 to 50 models through iterative steps. For the iterative process, up to 15 variables are defined as min-max boundary variables.

Table 1 and Fig. 5 summarize the design parameters for the optimal design process. The first variable to the third variable are design parameters for the stator winding. The number of rotor poles, stator slots and the number of windings for each slot per phase are determined by the winding configuration. The slot fill factor and torque

Table 1. Design Variables in DES.

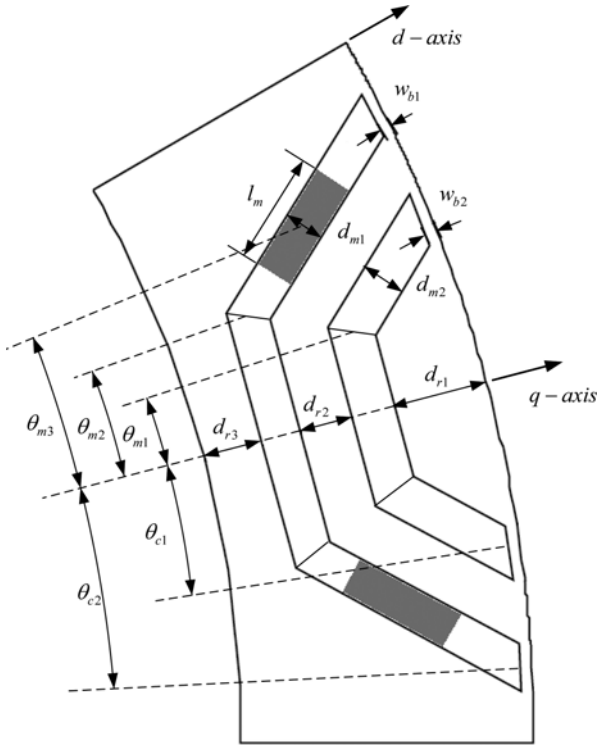| Design parameter in LPM	Minimum for DES	Maximum for DES
Number of rotor pole	4	16
Number of stator slot	6	48
Number of winding per slot	5	40
Axial stack length [mm]	50	80
Stator back iron depth	5	20
Ratio of slot height/width	0.5	2.5
Ratio of slot/(slot+tooth)	0.4	0.6
r_{ri}/r_{ro}	0.5	0.8
$(dm1+dm2)/(r_{ro}-r_{ri})$	0.2	0.5
dm1/(dm1+dm2)	0.3	0.5
dr1/(dr1+dr2+dr3)	0.15	0.4
dr2/(dr1+dr2+dr3)	0.2	0.4

Fig. 5. Design variables for the rotor core in DES.

pulsation due to the stator shape design, the back iron depth, slot height, and width are also design parameters in the LPM. These five variables are converged to satisfy the objective function in the DES method by iterating between the minimum and maximum value. For the purpose of minimizing the volume of the rotor core and permanent magnets using the objective function, six variables for the rotor core are used in the LPM. The inner diameter of the rotor core is decided by the ratio of the outer diameter to the inner diameter r_{ri}/r_{ro}. The permanent magnet thickness d_{m1}, d_{m2} and the bridge thickness w_{b2}, w_{b2} are decided by the ratio between two variables of magnet thickness and three variables of bridge thickness. Finally, the span ratio θ_m is optimized by the DES for minimizing the torque pulsation and the cogging torque.

Each iterative design is evaluated with the objective function of finding a better candidate. Each candidate design that meets all the requirements, such as the required power, is then evaluated for being a good design using the objective function.

$$Objective\ Function = \sqrt{k_1 \cdot I_a^a + k_2 \cdot generator\ cos\ st^2}\ (6)$$

The objective function in (6) can be configured by using a variety of quantitative evaluation criteria, including a permanent magnet (PM) flux linkage, efficiency, or a power factor. The weighting coefficients k_1 and k_2 are added to adjust the importance of multiple criteria in the penalty

function. For the 3 kW PMa-SynRG design, predicted minimal generator cost and stator ohmic losses are employed as the basis for the penalty function. In case of applying a lower number of k_1, the phase current will be increased and machine efficiency decreased. When the penalty function is set to 0.5 and k_1 and k_2, machine efficiency does not reach 94%. Therefore, k_1 is set to 0.6 and k_2 is 0.4 to obtain higher efficiency. The differential evolution program explores large multi-dimensional design space to achieve the best design. The optimization program is configured to find the design that minimizes the machine cost, while also keeping the efficiency and power factor as high as possible.

3.3. Iteration between LPM and FEA

Fig. 6 illustrates the flow chart of the optimal design process using the LPM and the FEA. In the optimal design process, the two-dimensional FEA software is used for fine tuning of the candidate machine's design using the LPM. The FEA verifies calculations of the PM flux linkage as well as the d and q-axis inductances, and then, compares with the results obtained from the LPM. The estimated saturation flux source ϕ_b of LPM and the rotor structures can be fixed until the LPM and the FEA predictions are converged. This convergence typically requires two to three iterations. Therefore, FEA simulation requires just two or three times iterations.

With the current source supply, the average output torque and torque ripple are analyzed. Material properties, such as the PM relative permeability, the PM flux density, and
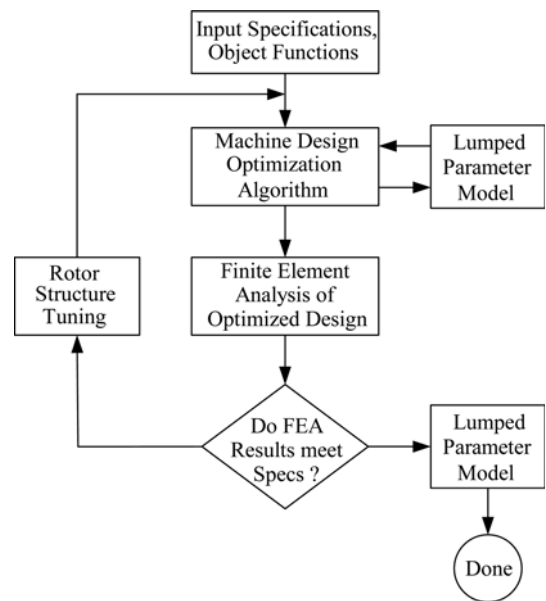

Fig. 6. Flow chart of optimization process using iterations of LPM and FEA programs.

the B-H curve of the core material, are inputted to the program. The PM flux linkage can be evaluated from the flux linkage of phase A, B and C without stator current excitations. Similarly, the cogging torque is obtained with only magnets being excited and the stator currents not being applied to the machine windings.
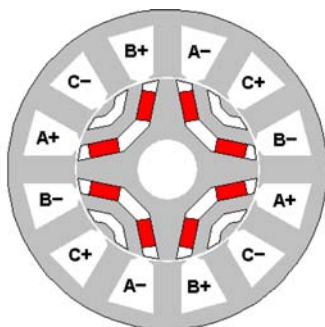
4. Simulation Results

4.1. Optimized results using LPM and DES

In the first process of optimization, selection of the rotor structure is performed. For high efficiency and performance, the first layer PM model is worse than the second layer PM model because the former has higher saturation and leakage flux on the bridge. Therefore, the first type has a larger power loss and it could not be survived by the objective function in the optimal design process. The final 3 kW rated power PMaSynRGs are found by the optimization process through the LPM and DES. Table 2 summarizes the machine parameters and output performances at a rated speed of 3,600 rpm. Two stator winding configurations based on distributed and concentrated are optimized with the second layer PM structure, respectively. Fig. 7 shows optimized PMa-SynRG of a 4-pole with

distributed windings and an 8-pole with concentrated windings. Since the stator winding is changed from the distributed winding to the concentrated winding, the number of stator slots/poles are chosen with 12/4 and 12/8, based on the limited stator outer diameter.
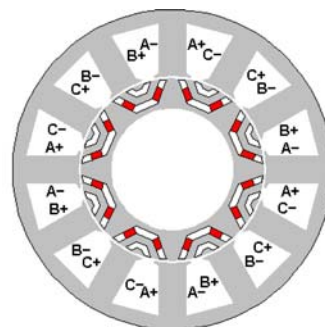
The stator current of each design is converged to 15A and the armature losses for the concentrated windings machine are reduced by 43% from 105.92 of the distributed winding to 60.27 of the concentrated winding. Moreover, the axial length of the machine and the total magnet mass in the concentrated winding are decreased by 17% and 40% compared to the distributed winding, respectively. As a result, the concentrated winding configuration yields lower cost than the distributed winding. The armature loss in the concentrated winding leads to better efficiency. Therefore, the concentrated windings machine has lower cost and better output characteristics than the optimized distributed windings machine.

4.2. Finite Element Analysis results

The FEA is performed to verify the optimized design obtained from the LPM and the DES to analyze output torque ripple and cogging torque. Flux line distributions of the distributed and the concentrated winding models are shown in Fig. 8.

The 2D FEA results demonstrate that the distributed winding machine has higher flux density distribution and it affect the stator and rotor core saturation. The concentrated winding machine is showing lower flux density characteristics in the same output torque with the distributed winding machine. Therefore, the concentrated winding machine has better performance for the saturation effects.

Fig. 9 illustrates the Back-EMF and the PM flux-linkage for the distributed and the concentrated winding from FEA. The rms value of the back-EMF for the concentrated winding model, calculated by the Fast Fourier Transform (FFT), is 82 V, whereas that for the LPM is

Table 2. Design Parameters and Results.

Stator Winding	Distributed	Concentrated
Number of Slots/poles	12/4	12/8
Series turns per phase	100	96
Rated current [Arms]	15.17	15.15
Stator outer diameter [mm]	190	190
Axial length [mm]	75	62
PM flux linkage [mWbrms]	83.77	56.62
Total magnet mass [Kg]	0.887	0.535
Core loss [W]	8.6	18.2
Armature loss [W]	105.92	60.27
Efficiency [%]	96.3	97.3

(a) PMa-SynRG with distributed windings

(b) PMa-SynRG with concentrated windings

Fig. 7. (Color online) PMa-SynRG with distributed and concentrated windings.

(a) Flux line distribution with distributed winding.

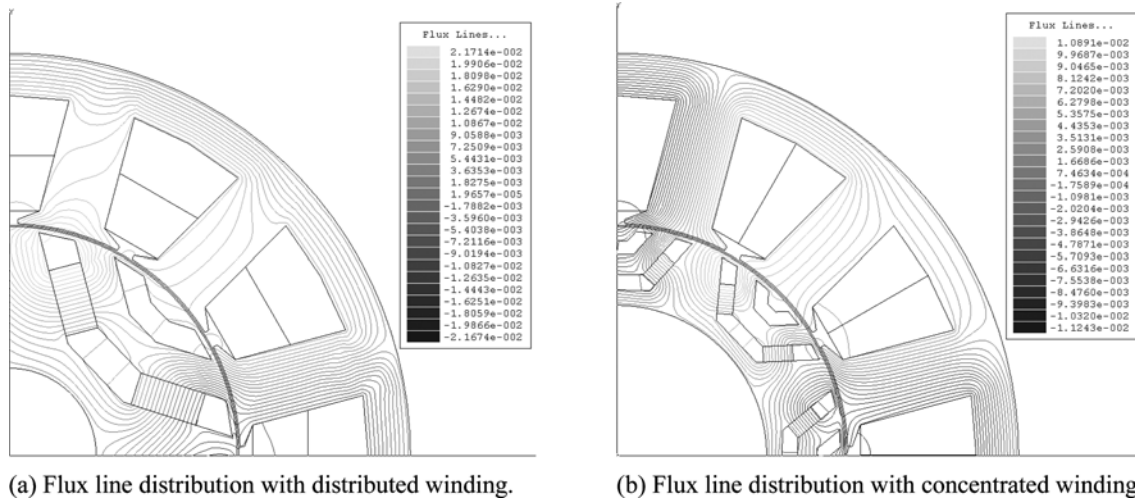(b) Flux line distribution with concentrated winding.

Fig. 8. Flux line distribution with distributed and concentrated winding.

Table 3. Comparisons between LPM and FEA Results.

Stator Winding	LPM	FEA	Error
Back-EMF [Vrms]	82	85.38	4%
PM-flux linkage [mWbrms]	53.8	56.62	5%

85.38 V. Therefore, it is seen that the error between the FEA and the LPM is around 4%. The rms value of the

PM flux linkage is calculated as 0.0538 Wb for the FEA, whereas the LPM result leads to 0.0566 Wb. As a result, the PM flux-linkage resulted from the LPM and the FEA are very close with only 5% error between them. Thus, it can be concluded that the optimized design results from the LPM is a close match with the FEA simulation results. The results obtained from the LPM and the FEA are summarized in Table 3.
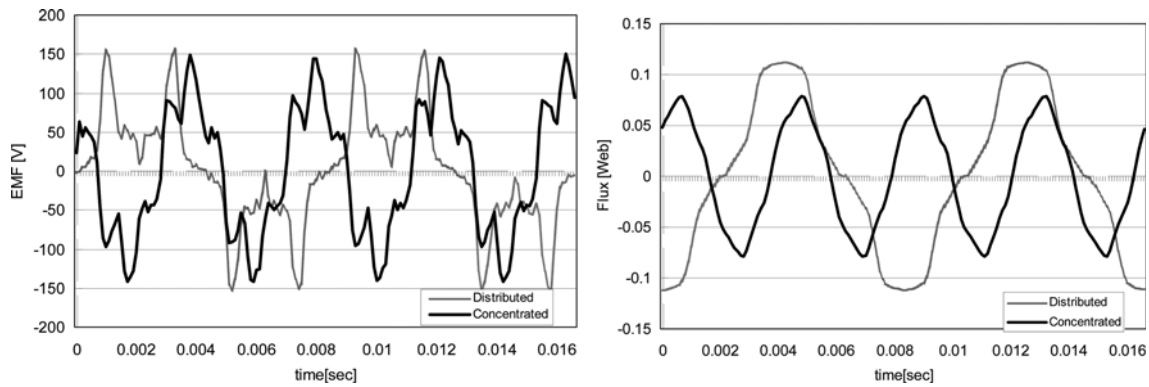

Fig. 9. Back-EMF and PM flux-linkage simulation results from FEA.
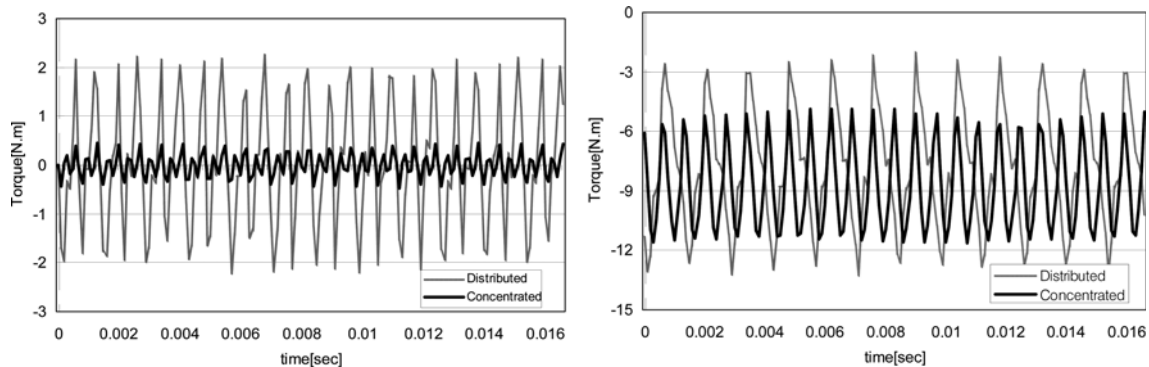

Fig. 10. Cogging torque and output torque simulation results from FEA.

Fig. 10 demonstrates the cogging torques and the output torque ripples for the distributed and the concentrated winding machines.

From the FEA simulation results, the cogging torque is reduced from 2 N.m for the distributed winding machine to 0.5 N.m for the concentrated winding machine. Also, the output torque ripple of 68.8% for the distributed winding machine is also decreased to 33.5% for the concentrated winding machine because the rotor pole number is doubled. From FEA results, the optimized design with the concentrated winding machine shows better output performance and lower torque ripple than distributed winding because of reducing the PM volume and increasing the rotor pole number, although both machines have the same level of back-EMF and PM flux linkage.

5. Experimental Results

The proposed PMa-SynRG with the concentrated stator winding was fabricated. Fig. 11 shows the stacked lamination stator core and rotor core fabricated in the lab, respectively.

The thickness of each lamination is 0.35 mm and the

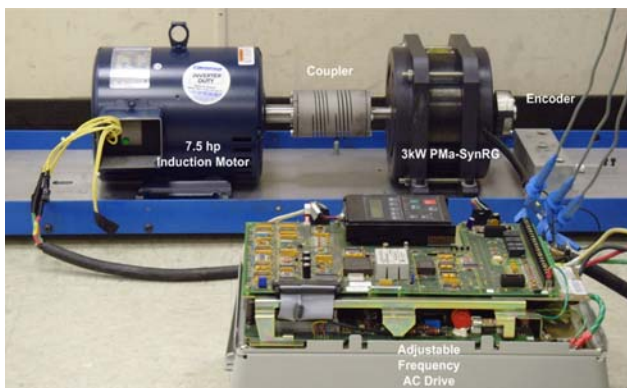**Fig. 11.** (Color online) Stacked lamination stator, rotor core and inserted PMs.

Fig. 12. (Color online) Experimental setup for the 3 kW PMa-SynRG.

total stack length is 65 mm. Therefore, 185 laminations are stacked and six points at the edge of the core are notched for welding. All stator slots are covered by isolation papers to isolate the coil and stator core. The number of turns per each stator slot and the total number of turns per each phase is 24 and 96, respectively. The estimated phase resistance is 0.175 ohm in the LPM and the measured value is 0.2 ohm. Therefore, the actual machine has 10% higher resistance because the volume of the end-turn is bigger than expected. The slot fill factor of the stator winding is set to 40% in the design process to consider the winding by hand.

Fig. 12 shows the experimental setup for the fabricated concentrated winding 3kW PMa-SynRG test bed.

A 7.5 hp three-phase induction motor is controlled by an adjustable frequency AC drive to run at 3,600 rpm. The fabricated 3 kW PMa-SynRG is coupled with the induction motor directly by a coupling. The supply frequency of the PMa-SynRG is 240 Hz because the PMa-SynRG has 8 rotor poles. The mechanical rotating position is detected by an encoder installed on the PMa-SynRG shaft. The 3 kW PMa-SynRG works as a generator with its phase conductors connected to a three-phase rectifier, in order to produce the dc-link output power.

5.1. Comparisons for Back-EMF

Experimental waveforms of the line-to-line and phase back-EMF are depicted in Fig. 13. In case the PMa-SynRG runs at 3,600 rpm, the peak value of the line-to-line back-EMF between phase A and B is around 150 V. The shape of the back-EMF waveforms is different because of the saturation effect in the experiment. Therefore, the experimental back-EMF waveform is close to the sin wave and
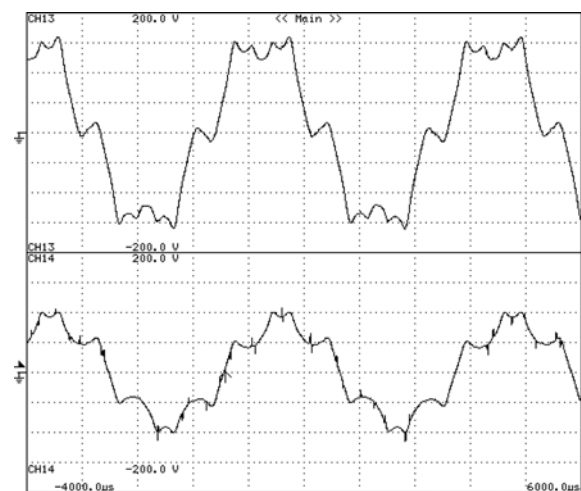

Fig. 13. Experimental results (a) line-to-line back-EMF (50 V/div, 1 ms/div) (b) phase back-EMF (50 V/div, 1 ms/div).

Table 4. Comparisons of the back-EMF from the experiment.

	LPM	FEA	Experimental
back-EMF [Vrms]	85.4	82	91.8

the peak value of the fundamental component is higher than the FEA simulation result.
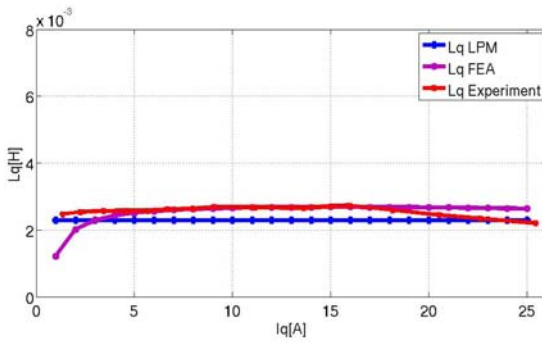
Each rotor pole has a uniform peak value indicating that each permanent magnet has equal remnant flux density B_r. The rms value of the back-EMF is 91.8 V, which is 7% higher than the FEA result. The smaller ripple in the back-EMF can yield bigger rms values and reduce the size of a dc-link capacitor or a dc-link inductor in rectifiers.

Table 6 summarizes the back-EMF design results from the LPM, the FEA and the experiments. The smaller ripple waveform of the back-EMF in the experiment can produce bigger rms value and reduce the size of the DC link reactor to rectify pure DC current or voltage. The rms value of the experimental result is 10 V higher than the FEA result because the adopted NdFeB magnet had a 10% higher magnetic flux density.
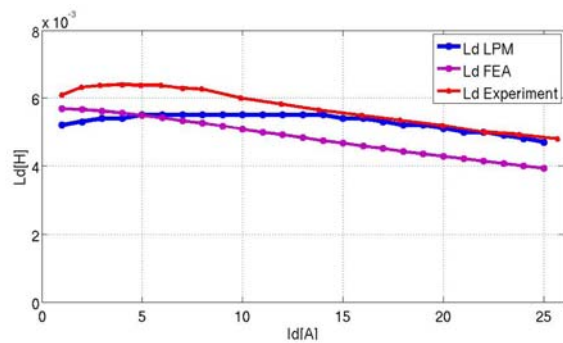
5.2. Comparisons for q and d-axis inductances

Experimental results and estimations for the d and q-axis inductances are illustrated in Fig. 14. The q-axis inductance measured by the experiment is close to the LPM and the FEA predictions.

The d-axis inductance measurements by the experiments are very close to the LPM predictions at the high current area. The FEA prediction plots have a similar trend with the experimental result, which is lower than the experimental result at overall currents because 2D FEA does not including end-turn of stator winding. At lower current ranges, the measured inductances are deviated from the LPM predictions, because of the uncertainty related to the low value of currents and voltages. However, at higher currents, the measurement plots follow the LPM predictions closely.

5.3. Experimental results for output power

In case the PWM gate signals for transistors are not fired, free-wheeling diodes in the IGBT conduct and this circuit work as a three-phase diode rectifier. In this case, the DC link voltage is the same as the peak value of the line-to-line input voltage. In the experiment, the three-phase voltage-fed PWM rectifier with load and no load conditions by diode rectifying are verified. The peak value of the line-to-line voltage is 150 V and the line-to-neutral voltage is 87 V when the induction motor runs at 3,600 rpm. Therefore, the DC link voltage is 150 V by three-phase diode rectifying at the no load condition, as shown in Fig. 15.

When the resistive load is connected to the DC link, phase currents are flowing through diodes and the output voltage is decreased from 150 V to 130 V. Fig. 16 shows the experimental waveforms of the DC link voltage and phase current with the load condition. It is seen that the
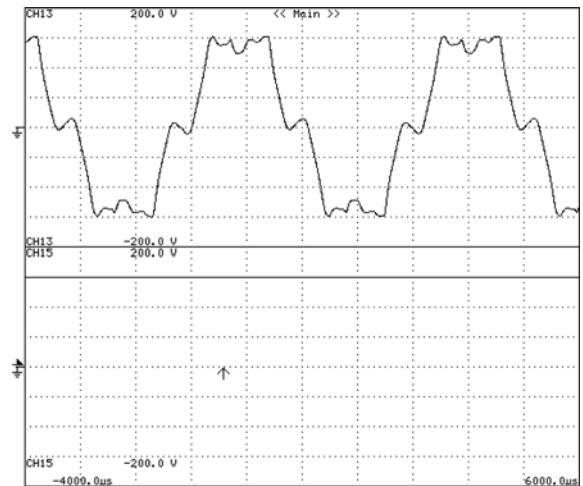

Fig. 15. Experimental waveforms of input voltage and DC link voltage with no load. Top to bottom: (a) line to line voltage (50 V/div, 1 ms/div) (b) DC link voltage (50 V/div, 1 ms/div).
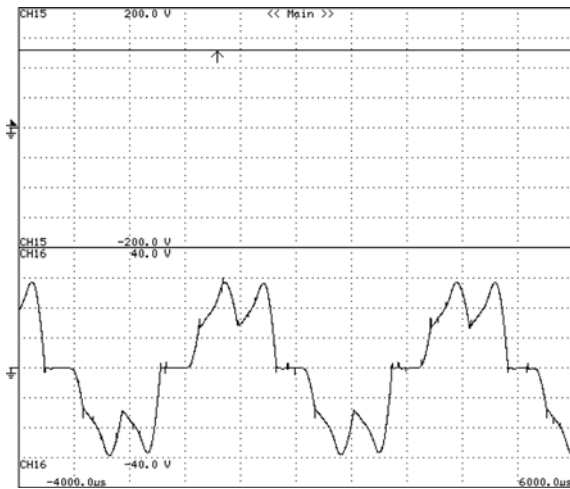

(a) q-axis inductance from LPM, FEA and experiment

(b) d-axis inductance from LPM, FEA and experiment

Fig. 14. (Color online) Measured q-axis and d-axis inductance characteristics.

Fig. 16. Experimental waveforms of DC link voltage and phase current with a load. Top to bottom: (a) DC link voltage (50 V/div, 1 ms/div) (b) phase current (10 A/div, 1 ms/div).

DC link voltage is 130 V. The 20 V voltage drop, in comparison with the no-load condition, is caused by generator phases and connection resistances. The peak value of the phase current is 30 A and the DC link current is around 25 A. Therefore, the maximum DC link power from the generator is 3,250 W and this result is close to the designed output power of the PMa-SynRG.

6. Conclusions

This paper investigates the optimal design of the 3 kW PMa-SynRG for the different rotor structures and stator winding configurations. The proposed design process can deliver the optimized design using the LPM and the DES supported by the FEA after several iterations. The proposed concentrated winding based PMa-SynRG can achieve better efficiency due to the 43% reduced armature loss. Moreover, the presented concentrated winding machine has lower cost than the distributed winding machine as a result of the 43% decreased magnet volume. With respect to output performances, the maximum generated power is designed to be equal for each winding configuration with wide CPSR. The output torque ripple is decreased from 68.8% to 33.5% and cogging torque is improved from 2 N.m to 0.5 N.m by using multiple poles and reduced magnet mass for the concentrated winding machine. Therefore, the optimized generator by the proposed optimal design process in this paper provides better performance and lower cost than the conventional distributed winding generator.

References

[1] A. M. El-Refaie, IET Electric Power Appl. **5**, 59 (2011).
[2] H. Murakami, Y. Honda, and H. Kiriyama, in Proc. IEEE Industry Applications Society Annual Meeting, Phoenix, USA (1999) pp. 840-845.
[3] Y. Kim, J. Magnetics **17**, 280 (2012).
[4] W. L. Soong, IEEE Trans. Ind. Appl. **38**, 1251 (2002).
[5] T. M. Jahns and V. Caliskan, IEEE Trans. Ind. Appl. **35**, 1347 (1999).
[6] P. Niazi, H. A. Toliyat, D. Cheong, and J. Kim, IEEE Trans. Ind. Appl. **43**, 542 (2007).
[7] L. Jian, G. Xu, Y. Gong, J. Song, J. Liang, and M. Chang, Progress In Electromagnetics Research **113**, 351 (2011).
[8] H. Jussila, P. Salminen, M. Niemela, and J. Pyrhonen, in Proc. Power Engineering, Energy and Electrical Drives, Terremolinos, Spain (2007) pp. 191-194.
[9] P. M. Lindh, H. K. Jussila, M. Niemela, A. Parviainen, and J. Pyrhonen, IEEE Trans. Magn. **45**, 2085 (2009).
[10] L. Chong and M. F. Rahman, IET Electric Power Appl. **4**, 249 (2010).
[11] P. Sergeant, F. D. Belie, and J. Melkebeek, IEEE Trans. Magn. **45**, 1756 (2009).
[12] K. I. Laskaris and A. G. Kladas, IEEE Trans. Ind. Electron. **57**, 138 (2010).
[13] D. G. Dorrell, M. Hsieh, M. Popescu, L. Evans, D. A. Station, and V. Grout, IEEE Trans. Ind. Electron. **58**, 3741 (2011).
[14] A. M. EL-Refaie and T. M. Jahns, IEEE Trans. Energy Conversion **23**, 53 (2008).
[15] M. Barcaro, A. Faggion, L. Sgarbossa, N. Bianchi, and S. Bolognani, IET Electric Power Appl. **4**, 537 (2010).
[16] A. S. Abdel-Khalik, S. M. Gadoue, M. I. Masoud, and B. W. Wiliams, IEEE Trans. Energy Conversion **26**, 501 (2011).